Land surface skin temperature climatology: benefitting from the strengths of satellite observations

2010 Environ. Res. Lett. 5 044004

(http://iopscience.iop.org/1748-9326/5/4/044004)

Environ. Res. Lett. **5** (2010) 044004 (13pp) doi:10.1088/1748-9326/5/4/044004

Land surface skin temperature climatology: benefitting from the strengths of satellite observations

Menglin Jin[1,3] **and Robert E Dickinson**[2]

[1] Department of Meteorology, San José State University, 1 Washington Square, San José, CA 95192-0104, USA
[2] Jackson School of Geosciences, The University of Texas at Austin, USA

E-mail: jin@met.sjsu.edu

Received 22 June 2010
Accepted for publication 17 September 2010
Published 4 November 2010
Online at stacks.iop.org/ERL/5/044004

Abstract
Surface skin temperature observations (T_{skin}), as obtained by satellite remote sensing, provide useful climatological information of high spatial resolution and global coverage that enhances the traditional ground observations of surface air temperature (T_{air}) and so, reveal new information about land surface characteristics. This letter analyzes nine years of moderate-resolution imaging spectroradiometer (MODIS) skin temperature observations to present monthly skin temperature diurnal, seasonal, and inter-annual variations at a 0.05° latitude/longitude grid over the global land surface and combines these measurements with other MODIS-based variables in an effort to understand the physical mechanisms responsible for T_{skin} variations. In particular, skin temperature variations are found to be closely related to vegetation cover, clouds, and water vapor, but to differ from 2 m surface T_{air} in terms of both physical meaning and magnitude. Therefore, the two temperatures (T_{skin} and T_{air}) are complementary in their contribution of valuable information to the study of climate change.

Keywords: land surface, skin temperature, remote sensing

1. Introduction

Global averaged land surface temperatures should be increasing with global warming (Jin and Dickinson 2002). They are determined by and respond to land surface–atmosphere interactions (Schmugge and Becker 1991, Jin *et al* 1997, 2005). Climatological data can be developed for two kinds of surface temperatures: 2 m surface air temperature (T_{air}) and the skin temperature (T_{skin}). How are these two surface temperatures related? Are they both needed? This letter addresses these questions by (a) assessing the differences between T_{skin} and T_{air} from their theoretical definitions and from recent global observations; and (b) addressing the strengths of satellite-based T_{skin} temperature data in terms of coverage, resolution, and consistency with other land and atmospheric data.

Various definitions of land surface temperature have been used in different research communities. Modeling, remote sensing, and boundary layer studies have used the same terminology ('land surface temperature') for different physical concepts. Such differences in usage have made it difficult to interpret data among interdisciplinary communities, and consequently have hindered scientific applications. Skin temperature terminology was previously clarified by Norman and Becker (1995). This letter provides additional clarification in the context of remote sensing and particularly in the context of climate change by assessing the differences between the T_{skin} and T_{air} for various spatial and temporal scales. Its references and their citations should complement this review in summarizing what is currently known about T_{skin} and T_{air}.

Surface temperatures are used for calculating heat and radiative fluxes, e.g., as a possible formulation:

$$F_{\uparrow} = \varepsilon \sigma T_{skin}^4 \quad (1)$$

[3] Author to whom any correspondence should be addressed.

$$\mathrm{SH} = C_{\mathrm{DH}} U (T_{\mathrm{aero}} - T_{\mathrm{air}}) \quad (2)$$

$$\mathrm{LE} = C_{\mathrm{DE}} U (q^{*}_{\mathrm{skin}} - q_{\mathrm{air}}) \quad (3)$$

where $F_{\uparrow}$ is upwelling longwave radiation, SH and LE are sensible and latent heat fluxes respectively, σ is the Stefan–Boltzmann constant, ε is surface spectrally averaged emissivity, U is wind speed, and C_{DH} and C_{DE} are bulk transfer coefficients for heat and moisture, respectively. T_{air} is the air temperature at the reference (shelter) height and T_{aero} is the aerodynamic temperature discussed further in section 3 and is related to T_{skin}. q^{*}_{skin} is the saturated specific humidity at T_{skin} and q_{air} is specific humidity at the same reference level as T_{aero}.

For a given region, the governing equation for land surface energy balance is:

$$(1-\alpha)S_{\downarrow} + F_{\downarrow} - F_{\uparrow} - \mathrm{SH} - \mathrm{LE} - G = 0 \quad (4)$$

where α is the surface albedo, $S_{\downarrow}$ is the surface insolation, $F_{\downarrow}$ is downward longwave radiation from atmosphere, and G is the ground heat flux. The calculation of heat fluxes and surface radiation terms in equation (4) depends on T_{skin} and other physical properties such as albedo (α) and emissivity (ε).

The term T_{skin} differs from T_{air} in its physical meaning, magnitude, and measurement techniques. As such, it provides additional information on land surface radiation properties because it is closely determined by surface longwave emissions, as shown in equation (1). Therefore, it is necessary to analyze the climatology of T_{skin} as distinct from that of T_{air}.

This letter addresses the issues associated with the use of T_{skin} by focusing on four specific but relevant topics: section 2 examines the different physical meanings of T_{skin} and T_{air}; section 3 describes the data used; and section 4 provides a climatology of T_{skin} as observed from the recent moderate-resolution imaging spectroradiometer (MODIS) instrument and compares this data with T_{air} data obtained from ground observations and NCEP reanalysis. A discussion as to the difficulties that hamper the use of T_{skin} is given in section 5 followed by final recommendations for future directions on this topic in section 6.

2. Definitions

2.1. Surface temperature

'Surface temperature' is, by itself, vague and may refer to T_{skin}, T_{air}, or T_{aero}, depending on the underlying physical principles of their measurement. This section defines various surface temperature measurements used in calculating land surface heat fluxes and radiation transfer processes, as presented in equations (1)–(3), following the previous overview of Norman and Becker (1995).

2.2. Skin temperature (T_{skin})

The term 'skin temperature' has been used for 'radiometric surface temperature' (Jin *et al* 1997). It can be measured by either a hand-held or aircraft-mounted radiation thermometer, as derived from upward longwave radiation based on the Stefan–Boltzmann law (Holmes 1969, Oke 1987), or retrieved from satellite observations and mapped over large areas, after removing the effects of atmospheric attenuation on satellite-measured radiances (Saunders 1967, Anding and Kauth 1970, Sobrino *et al* 1994, Stephens 1994, Ulivieri *et al* 1994, Prata 1993). The retrieval techniques for obtaining T_{skin} from satellite measurements for land applications have developed substantially in the last two decades (Price 1984). The accuracy of many T_{skin} algorithms has been improved to within 0.5–1°C for field measurements and for satellite observations under clear sky conditions (Becker and Li 1995, Wan and Dozier 1996, Coll *et al* 1994).

The definition of T_{skin} in satellite remote sensing is based on Planck's law. Radiances measured by satellite sensors observing the earth surface consist of both atmospheric and land surface radiation. The surface radiation at a specific wavelength gives the brightness surface temperature, defined as:

$$T^{\mathrm{b}}_{\mathrm{skin}} = B^{-1}_{\lambda}(L_{\uparrow}) \quad (5)$$

where $L_{\uparrow}$ is the radiance measured by the radiometer, after corrections for atmospheric and emissivity effects, and B^{-1} is the inverse of Planck's law $B_{\lambda}(T)$. Planck's law gives dependence on temperature of the radiative emission from a black body, i.e., surface spectral emissivity $\varepsilon_{\lambda} = 1$. Since the land surface is typically not a black body, equation (5) needs to be modified to account for variations in ε_{λ} (e.g., Li and Becker 1993):

$$T^{\mathrm{b}}_{\mathrm{skin}} = B^{-1}[(L_{\uparrow} - (1-\varepsilon_{\lambda})L_{\downarrow})/\varepsilon_{\lambda}] \quad (6)$$

where $L_{\downarrow}$ is the downward radiance from the atmosphere. For a homogeneous surface, the temperature from this definition is equal to the thermodynamic temperature of the surface (Norman and Becker 1995). Because the land surface has heterogeneous emissivity, many retrieval algorithms have used the concept of effective emissivity at the pixel level (Prata *et al* 1995, Schmugge *et al* 1998).

Climate models have generally used the Stefan–Boltzmann law, i.e., the integrated version of equation (6), to calculate $F_{\downarrow}$ (i.e., equation (1)). Errors in assuming ε to be some constant value are common in both formulations (equations (1) and (6)) because a correct value for ε is not easily available for large (frequently heterogeneous) surfaces (Jin and Liang 2006). Moreover, satellite-measured radiances correspond to the instantaneous field of view of the instrument and include part of the surrounding sky flux. For this reason, a satellite-based definition of T_{skin} (e.g., $T^{\mathrm{b}}_{\mathrm{skin}}$) is ideally used for measurements over a small area or for calculating fluxes where the emissivity is measured, inferred or otherwise estimated. In the remainder of this letter, T_{skin} is the radiometric temperature derived from the inverse of the Planck's function (namely, $T^{\mathrm{b}}_{\mathrm{skin}}$ in equation (6)).

2.3. Surface air temperature (T_{air})

Traditionally, thermodynamic temperature (or equivalently kinetic temperature) has been measured by an *in situ* thermometer in a shelter at 1.5–2 m and with good thermal contact with the air. This is the surface air temperature or, more accurately, air temperature at shelter height. This near-surface air temperature is correlated with T_{skin} but can differ

depending on land cover or sky conditions; differences may be large, e.g., for sparsely vegetated areas with most of the net radiation balanced by sensible heat flux (Sun and Mahrt 1995, Jin *et al* 1997). Norman and Becker (1995) summarize the conceptual differences between thermodynamic and kinetic temperature that are here taken to be essentially equivalent.

2.4. Aerodynamic temperature (T_{aero})

Another surface temperature that is related to T_{skin} and T_{air} is the aerodynamic temperature, i.e., the temperature at the height of roughness length for heat. Unlike roughness length for momentum, where the surface wind speed reduces to zero due to surface friction, roughness length for heat is the level heat transfer at zero. In an aerodynamically smooth flow, roughness length is independent of surface geometry and wind speed. However, for an aerodynamically rough flow, roughness length varies with surface geometry (Garratt 1992, p 87).

Aerodynamic temperature may fall between surface air and radiometric skin temperature, but can be quite different from the latter. Typically, the skin temperature can be 2–6 K higher than the aerodynamic temperature at midday, and lower than the aerodynamic temperature at night (Sun and Mahrt 1995). Some models, however, have approximated the surface radiative temperature by the aerodynamic temperature (Huband and Monteith 1986) while others including BATS (biosphere–atmosphere transfer scheme, Dickinson *et al* 1986, 1993) and CLM (community land model, Oleson *et al* 2008) have assumed a thin boundary layer over the leaves or soil where molecular diffusion generates the difference between T_{aero} and T_{skin}.

3. Data

Monthly observations of skin temperature, albedo, and land cover data measured by MODIS Terra (Wan and Dozier 1996, Schaaf *et al* 2002, Gao *et al* 2005, Friedl *et al* 2002) from April 2000–December 2008 are used to analyze the climatology of skin temperature and how it relates to surface properties. Details of skin temperature collection four process and validation can be found at Wan (2008) and Wan and Li (2008), or the user's guide at (www.icess.ucsb.edu/modis/LstUsrGuide/MODIS_LST_products_Users_guide_C5.pdf). The MODIS data (Collection 5) is at 0.05° latitude/longitude grid. T_{skin} data is only retrieved on clear days. The daytime and nighttime T_{skin} values in MOD11C3 are averaged from the daytime and nighttime LST values in the daily T_{skin} product (MOD11C1) in clear days only. The daytime T_{skin} in MOD11C1 is around 10:30 am local solar time and the nighttime T_{skin} is around 10:30 pm local solar time. The observation time may differ by 90 min in low latitude regions or up to several hours in high latitude regions. Local solar time is equal to coordinated universal time (UTC) + longitude (in degrees)/15.

In addition, water vapor and cloud observations from MODIS (Gao *et al* 2003, King *et al* 2003, Platnick *et al* 2003) are also used to examine the connections between surface temperature and atmospheric conditions.

Observed surface air temperatures are provided by the global historical climatological network (GHCN, for details see www.ncdc.noaa.gov/temp-and-precip/ghcn-gridded-temp.html, and also Peterson and Russell 1997, Peterson *et al* 1998, Free *et al* 2004). These datasets were created from 2 m observations at World Meteorological Organization (WMO) observation sites (namely, screen-level shelters). In order to make the limited coverage of the data sites as useful as possible, an anomaly method (AM) is implemented which first calculates station averages for a selected duration (1961–1990, in this case) and then departures by subtracting this average from the raw data. The data set is given in 5 × 5 degree grid boxes, as calculated from station anomalies for all adjusted stations falling within the 5 × 5 degree box. An adjusted station is one with at least 25 years of data during the 1961–1990 period. For stations which are too new to be adjusted, anomalies were calculated from the raw station data using the same AM approach.

In addition to GHCN, daily T_{skin} and T_{air} data from the atmospheric radiation measurement (ARM) program are used to reveal the differences between T_{skin} and T_{air}. The ARM site used was from surface meteorological observation station (SMOS) at E13: Lamont, OK (36.605°N, 97.485°W, altitude 318 m). T_{air} is measured at 2 m height with 30 min intervals. Two days, 1 January 2006 and 1 July 2006 were analyzed. Corresponding T_{skin} data is obtained from the same site. T_{skin} was named as ground surface infrared temperature in the data set and was observed at 10 m and remove atmosphere effects. The interval of T_{skin} is 60 s.

4. Results

4.1. T_{skin} versus T_{air}

Why do we need to use T_{skin}, when T_{air} data have been obtained for decades with much effort going in to constructing a data set for use (Peterson and Russell 1997, Peterson *et al* 1998)? Figure 1 partly answers this question by showing that T_{skin} and T_{air} are significantly different in terms of magnitude, response to atmospheric conditions, and diurnal phase. On 1 July 2006 at Lamont, OK (figure 1(b); 36.605°N, 97.485°W), which was a clear day except for clouds flying across the observation site during the afternoon, T_{skin} was higher than T_{air} during the daytime with the maximum T_{skin} of 50 °C around local noon while T_{air} was only 35 °C. This 15 °C difference is significant for heat and moisture fluxes. At night, T_{skin} was consistently lower than T_{air} by about 3 °C. The reasons for the T_{skin} and T_{air} differences are complex. Clouds may be one of the major reasons. For example, in the afternoon of 1 January 2006 (figure 1(a)), T_{skin} was lower than T_{air} when clouds were present, but during the morning T_{skin} was higher. At night on the same day, T_{skin} was lower than T_{air} by about 4 °C. In addition, in both the January and July cases (figures 1(a) and (b)), the diurnal phase of T_{air} shifted to later in the afternoon compared to that of T_{skin}, because the skin surface warmed up first as a result of absorbing surface insolation and then heated the near surface air.

Another reason for studying T_{skin} is that T_{skin} observations provide more coverage than T_{air}. High spatial resolution is

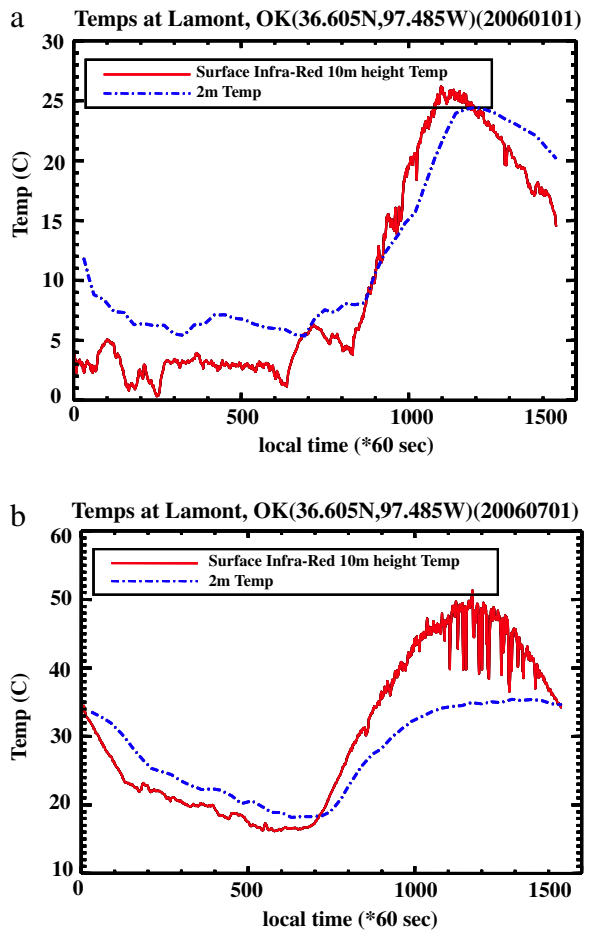

Figure 1. Skin temperature and air temperature from the Arm Lamont, OK site. Site location is 36.605°N, 97.485°W.

one of the key strengths of satellite data, and it can reveal tremendous details over the globe. Inter-annual variations of T_{skin} (January 2006 minus January 2001) provide an example of how much T_{skin} can vary between different years (figure 2(a)). Over eastern USA, January was much warmer in 2006 than in January 2001, with much of this region 10 °C higher than in 2001. By contrast, Europe and Canada had a cold winter in 2006 with surface temperatures 10 °C lower than those of 2001. In addition, the southern part of Greenland, South Africa (∼20°S), Sahara deserts, and Australia all experienced colder winters in January 2001 than in January 2006. Similar but weaker inter-annual variations of T_{air} occur (figure 2(b)). Since the T_{air} observations over the globe are not uniformly distributed (one of the limits of T_{air} observations), many areas cannot have observations over T_{air}. Therefore, solely relying on T_{air} data maybe misleading to accurate land surface change over the globe. In general, the major patterns of T_{air} are consistent with those of T_{skin}, although details differ.

4.2. Global distribution of skin temperature

Polar-orbiting satellites monitor global distributions of specific variables. For remotely accessible regions such as Greenland and Antarctica, these measurements provide critical information that is often missing with *in situ* ground observations. The spatial and temporal variability of T_{skin} is similar to that of T_{air}. In the following paragraphs, we describe and quantify this variability.

The global distribution of T_{skin} varies with the surface insolation depending on the solar zenith angle (figure 3). The north-polar region in January has its minimum T_{skin} in Greenland with its monthly average around 220 K. Temperatures increase southward, with the warmest regions in January occurring over the deserts in South Africa, tropical Africa, South America, and Australia, where the temperature is above 320 K (figure 3(a)). In July, Greenland has a skin temperature of about 260 K in its central glacier areas, but up to 290 K at the edges where the surface is free of snow and ice (figure 3(b)). These margins are important for climate change as snowmelt can cause a positive feedback that promotes the melting of ice sheets and glaciers. From January to July the maximum surface insolation has shifted from the Southern Hemisphere to the Northern Hemisphere. Correspondingly, land masses receive the most amount of solar energy in summer, and from the equator to 30°N reach daytime temperatures of about 320 K. Much of these areas are desert with high albedo and low soil moisture. The coldest region over land in July is the central Antarctic plateau with skin temperature below 210 K. Depending on details of the surface and of the surface boundary layer processes, the minimum skin temperatures are generally colder than air temperatures and maximum daytime values warmer.

4.3. Diurnal variations

All land surfaces show significant diurnal variations[4] of T_{skin} (figure 4). The desert regions in the sub-tropics (i.e., the Sahara, southwestern USA, southern Africa, Australia, and India) have the highest daytime skin temperatures up to 310–320 K (figure 4(a)) as well as at the highest nighttime temperatures up to 290–300 K (figure 4(b)), and the largest diurnal range (daytime minus nighttime as large as by 20–25 °C, figure 4(c)). A diurnal range above 25 °C is seen over some mountainous regions, in particular, the Tibetan Plateau. By contrast, most forest regions have low skin temperature diurnal range. For example, the T_{skin} diurnal range of the Amazon is only 2.5–5 °C. Other regions with small diurnal range (values less than 5 °C) are cold, snow-covered regions including Greenland and Antarctica.

Both daytime and nighttime T_{skin} have substantial seasonality (figure 5), with their maxima values occurring in Northern Hemisphere summer months (June, July, and August (JJA)) and minima in the winter months (December, January, and February (DJF)) as a result of solar insolation. The peaks of global averaged, monthly mean T_{skin} are all above 295 K and the minima below 275 K. Furthermore, inter-annual variations are also evident; in 2005 JJA global T_{skin} was about 1 °C higher

[4] Note that here the observed MODIS T_{skin} used were taken by NASA MODIS on Terra platform at 10:30 am and 10:30 pm, respectively. Its absolute range is likely to be smaller than the true diurnal range, i.e., the maximum minus the minimum skin temperatures. Nevertheless, the spatial pattern of this diurnal range should still be informative.

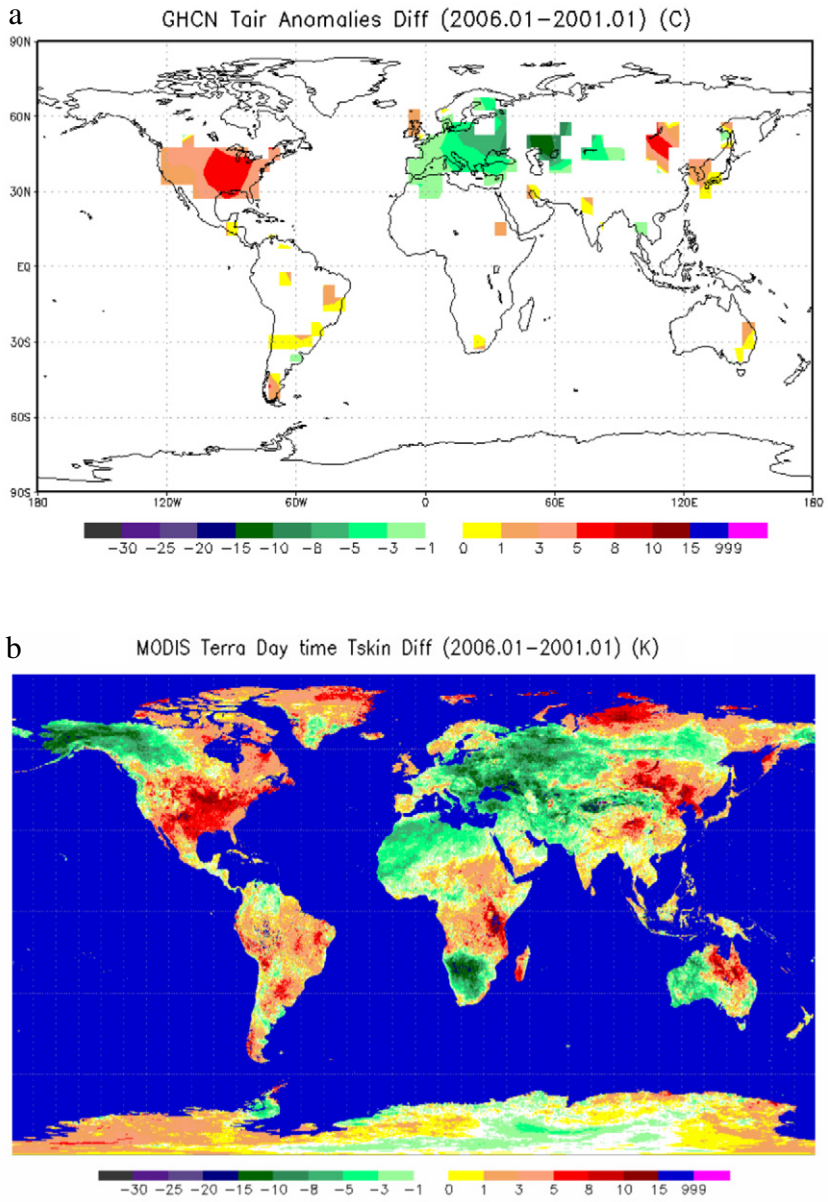

Figure 2. Inter-annual variability for (a) surface air temperature and (b) surface skin temperature. Skin temperature is from MODIS daytime observation at 0.05° latitude/longitude, and air temperature is monthly mean from GHCN.

than those in 2001–2004. Similarly, the year 2006 was the warmest winter for the period 2000–2006.

Scale is critical in climate study. The features or even the signs can be different from one scale to another. Therefore, to get a complete picture of a variable, one needs to examine it at different spatial or temporal scales. Figures provide an example of T_{skin} at global land scale (figure 6(a)), at continental scales (figures 6(b) and (c)), and at regional scales (figure 6(d)).

The smaller spatial scales (individual continents or land masses) have larger seasonality. For example, as shown in figure 6(b), the T_{skin} differences between July and January in USA can be 25 °C (295 minus 270 K), but at global scale the T_{skin} seasonal range (figure 6(a)) is only 14 °C (292 minus 278 K). In addition, different land surfaces have distinct seasonality. For example, Greenland (figure 6(d)) has a seasonal change of about 15 °C, while Africa (figure 6(c)) has a seasonal range of up to 40 °C.

4.4. T_{skin} versus land cover

One strength of satellite MODIS data is that MODIS provides simultaneous measurements for many land and atmospheric variables, and so facilitates the combination of T_{skin} data with other variables to study the mechanisms responsible for its changes. For example, land cover data helps to interpret how T_{skin} varies as a function of the underlying land surface vegetation coverage.

Land cover maps are provided by the MODIS land cover group and can be downloaded from www.geog.bu.edu (figure 7). Evidently, skin temperature is related to land cover. For example, desert regions have higher surface temperature

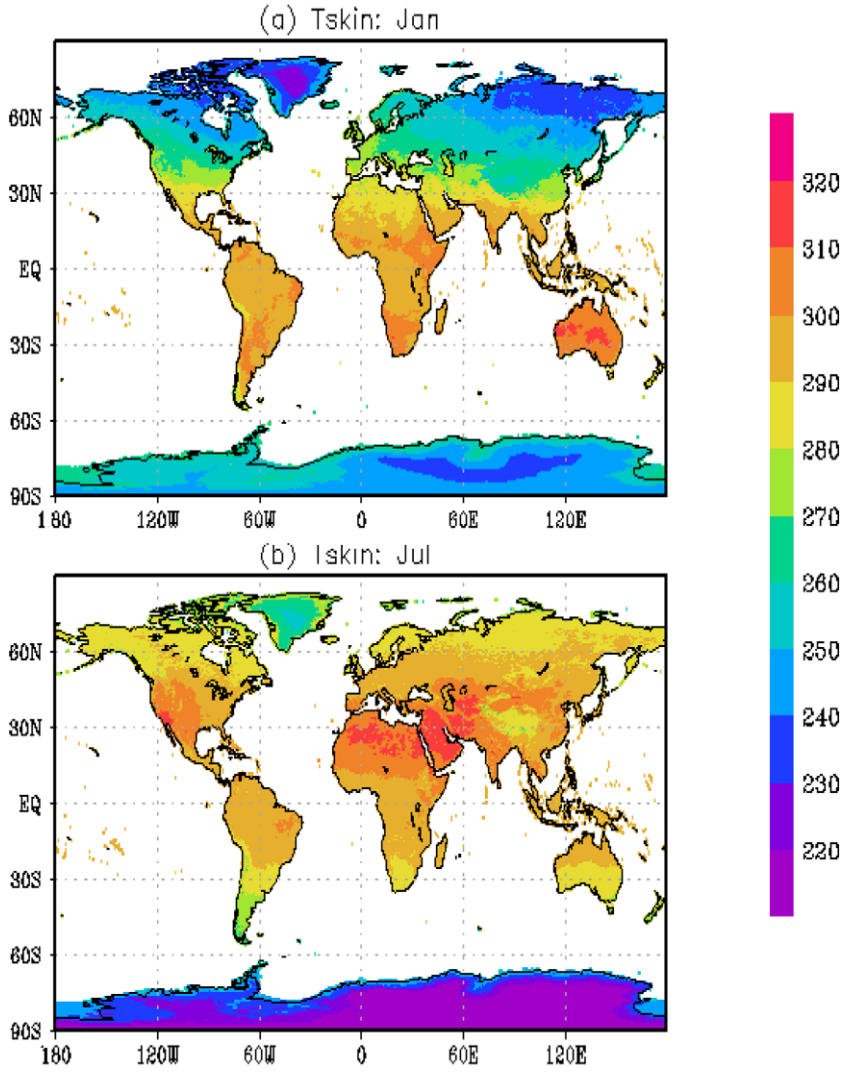

Figure 3. Global distribution of monthly mean skin temperature (a) January and (b) July. Data is from MODIS monthly averaged from 2001–2008. Resolution is 0.05 km. Unit is K. Data is from the Terra platform daytime orbits (10:30 am) for a given area.

than the surrounding non-desert regions, because deserts have little soil moisture but large surface insolation. The absorbed solar radiative energy is used to heat up the surface instead of giving evaporation.

Figure 8 examines the relationship of skin temperature to land cover for four-month averages of $T_{\rm skin}$ (January, April, July, and October) over the globe for each type of land cover. The minimum skin temperature is for land cover type 15 'snow and ice'. Its monthly means are 249.99 K, 233.03 K, 230.85 K and 237.07 K for January, April, July, and October respectively. The maximum skin temperature is for land cover type 16 'barren or sparsely vegetated', with values as 290.28 K, 307.13 K, 314.78 K, and 306.80 K for January, April, July, and October respectively. In addition, the largest seasonal difference occurs for land cover type 3 'evergreen needleleaf forest', varying from 242.48 K in January to 296.13 K in July (total difference is about 55 °C). Also interestingly, 'savannas' (land cover type 9) have a larger $T_{\rm skin}$ in October (308.54 K) than in July, and their January and July $T_{\rm skin}$ are almost the same (∼304 K). Furthermore, 'evergreen broad leaf forest' (land cover type 2), 'woody savannas' (land cover type 8) and 'savannas' (land cover type 9) show little seasonal differences between January and July, while other land cover types have clear seasonal variations.

4.5. T_{skin} versus surface albedo

Skin temperature is determined in part by surface albedo, i.e., how much surface insolation is reflected back to space. Figure 9 shows a clear relationship between yearly averaged $T_{\rm skin}$ and land surface albedo. In general, albedo decreases from Northern Hemisphere winter to Northern Hemisphere summer, with the peak in February and March when the surface snow cover reaches a maximum. Global, year-averaged skin temperature has the opposite phase with surface albedo, namely, warm in July and cold in December and January. Another example of $T_{\rm skin}$ and surface albedo over Greenland across 70°N (figure 10) clearly shows that $T_{\rm skin}$ decreases with the increase of albedo from the edges to the center. Even along the same latitude (70°N), at the edge $T_{\rm skin}$ is above 280 K at 50°W and 27°W, suggesting that the melt of surface snow cover at the edges during summer has an evident influence.

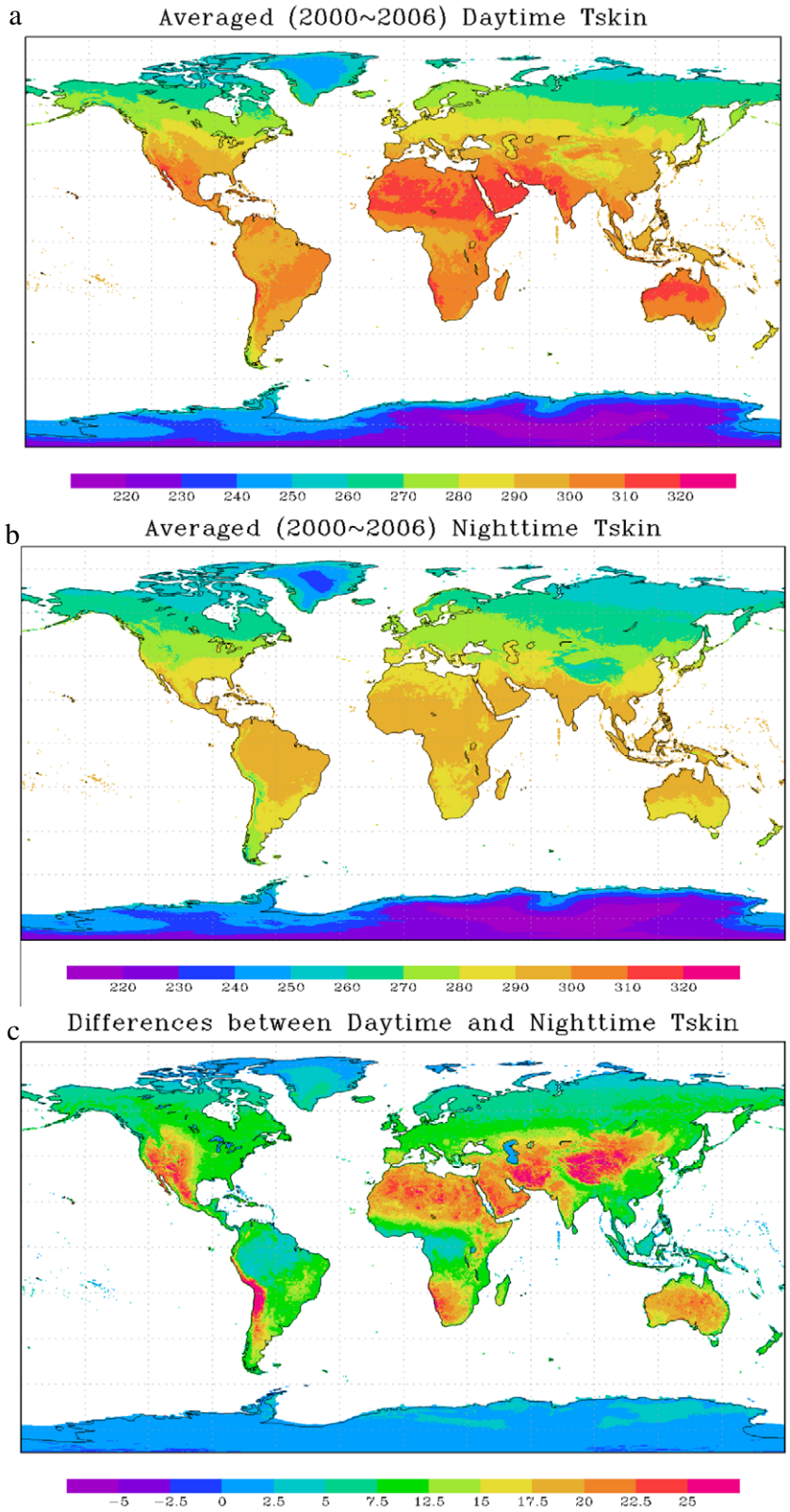

Figure 4. Six-year (2001–2006) averaged MODIS skin temperature measured (a) daytime at 10:30 am, (b) nighttime at 10:30 pm, and (c) daytime minus nighttime.

Both T_{skin} versus land cover and T_{skin} versus albedo relationships show that in addition to the changes in air temperature and insolation, T_{skin} also depends on vegetation health, canopy depth, and soil wetness. Because of such interdependencies, it may be difficult to relate changes in T_{skin} to those in T_{air} such as seen as global warming. For example, shifts in precipitation patterns will have a larger influence in one area than in another. Therefore, one may gain more

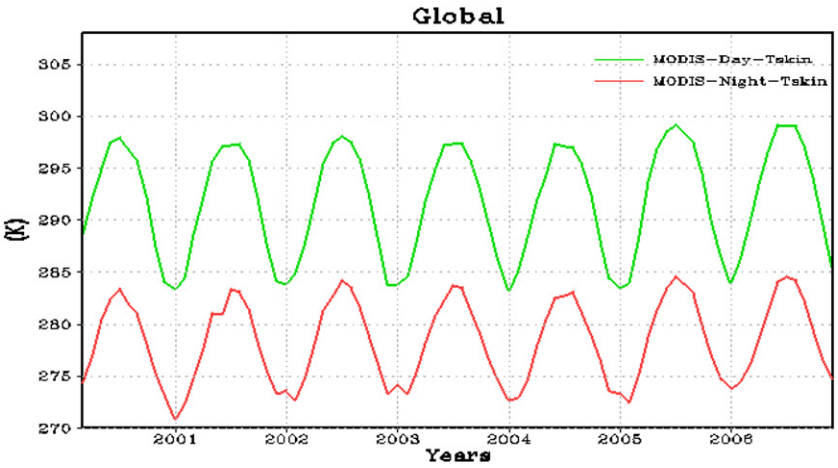

Figure 5. Daytime and nighttime skin temperature seasonality. Data is based on 2001–2006 monthly mean MODIS observations at 10:30 am and 10:30 pm respectively.

understanding with the use of T_{skin} in global climate change studies.

4.6. T_{skin} versus vegetation

Vegetation information is represented by the enhanced vegetation index (EVI) from MODIS remote sensing. In figure 11, EVI less than 0 is related to water or snow surfaces. For EVI from 0 to 0.9, which is the valid vegetation-covered region, T_{skin} almost linearly decreases with the increase of EVI, suggesting that more vegetation would reduce surface skin temperature. Such a decrease is partly because there is more vegetation, more evaportranspiration, and therefore less heat is used to warm up the surface. On the other hand, since T_{skin} is observed from space, larger EVI represents dense, forest area where T_{skin} is mainly the canopy top temperature. In addition, for the studied region 40–60°N, 80–120°W, T_{skin} is the highest, upto 265 K, when EVI is 0.1.

4.7. T_{skin} versus atmospheric conditions

MODIS measures land and atmospheric conditions at the same time over quite a few years of observations, facilitating the study of land surface–atmosphere interactions. For example, water vapor is closely related to T_{skin} (figure 12), as expected from many earlier studies relating surface air temperature and water vapor. Both water vapor and T_{skin} show the same seasonality—peaking in June, July, and August and minimizing in November, December, January, and February. The higher the surface skin temperature, the more water vapor can be contained in the atmospheric column. (But for desert regions less water vapor is transported or evaporated so there would be less water vapor than in other regions of similar temperatures.) In addition to water vapor, global averaged cloud optical thickness also shows similar seasonality to that of T_{skin} over land (figure 13). Further clarification of these interactions should shed light on what causes land surface

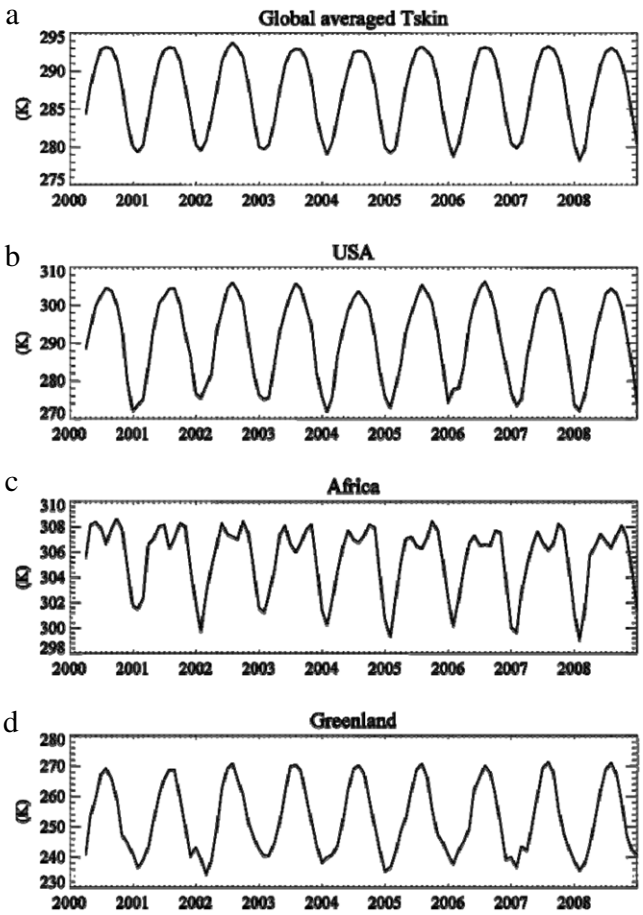

Figure 6. Seasonality for various regions (a) global land surface, (b) USA (Lat: 30°–50°N, Lon: 70°–125°N); (c) Africa (Lat: 10°–30°N, Lon: 20°–55°E); and (d) Greenland (Lat: 60°–80°N, Lon: 20°–60°E). Data is from MODIS.

temperatures to change over a given region, specifically, to what extent are the changes a result of changes of local land cover or land use and to what extent they are due to changes of large-scale dynamics.

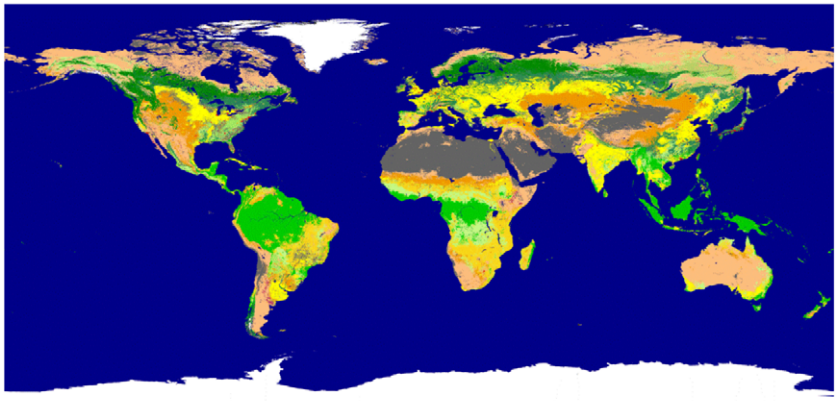

MOD12C1 Land_Cover_Type_1 (IGBP)		
Land Cover	**Class**	**Color**
Fill Value	255	
Water	0	
Evergreen Needleleaf Forest	1	
Evergreen Broadleaf Forest	2	
Deciduous Needleleaf Forest	3	
Deciduous Broadleaf Forest	4	
Mixed Forest	5	
Closed Shrubland	6	
Open Shrubland	7	
Woody Savannas	8	
Savannas	9	
Grasslands	10	
Permanent Wetlands	11	
Croplands	12	
Urban and Built-Up	13	
Cropland/Natural Vegetation Mosaic	14	
Snow and Ice	15	
Barren or Sparsely Vegetated	16	
Unclassified	254	

Figure 7. Land cover derived from MODIS (image is copied from www.bu.edu).

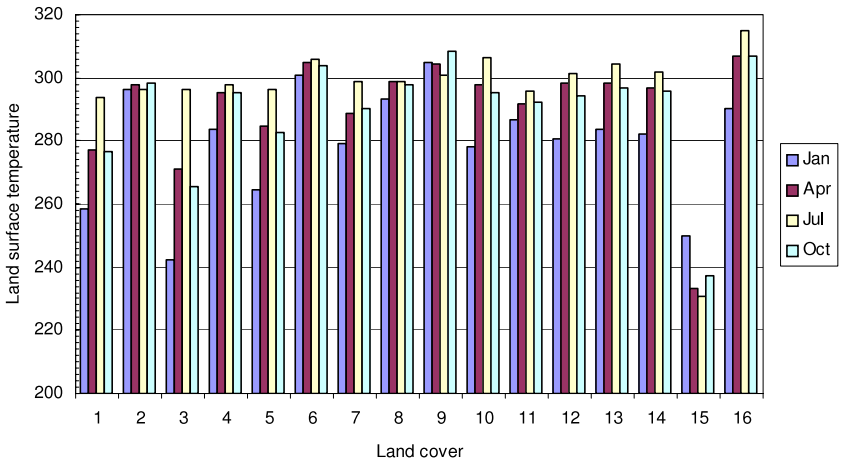

Figure 8. MODIS observed global mean LST as a function of land cover. (1) Evergreen needleleaf forest; (2) evergreen broadleaf forest; (3) deciduous needleleaf forest; (4) deciduous broadleaf forest; (5) mixed forest; (6) closed shrubland; (7) open shrubland; (8) woody savannas; (9) savannas; (10) grassland; (11) permanent wetland; (12) croplands; (13) urban and built-up; (14) cropland/natural vegetation mosaic; (15) snow and ice; (16) barren or sparsely vegetated.

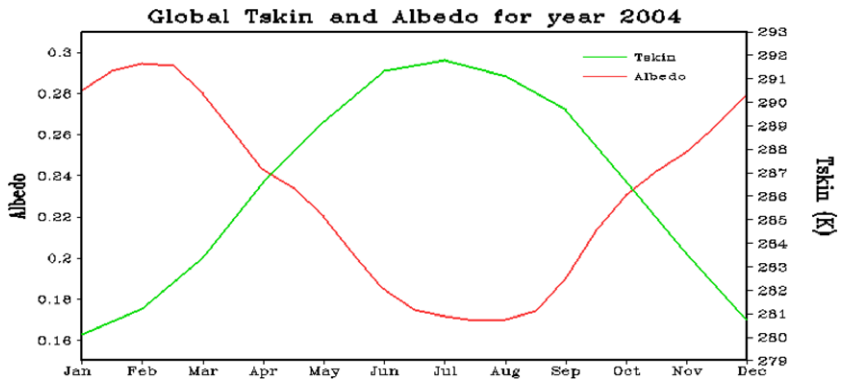

Figure 9. Global averaged T_{skin} versus surface albedo for months of the year 2004. The T_{skin} and albedo observations are from MODIS Terra measurements.

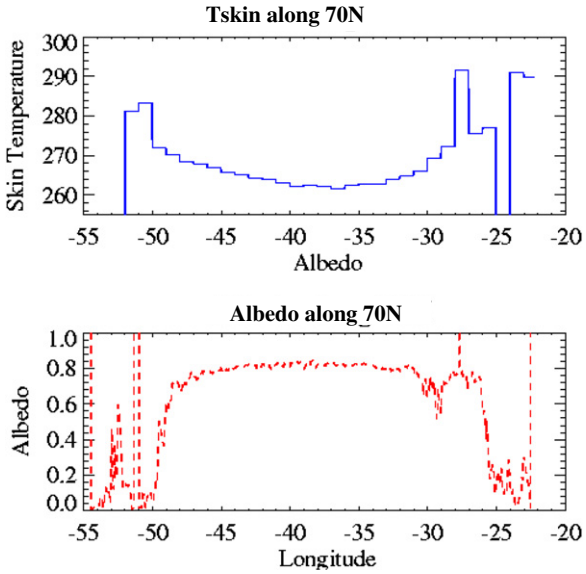

Figure 10. MODIS albedo and skin temperature for Greenland along 70°N.

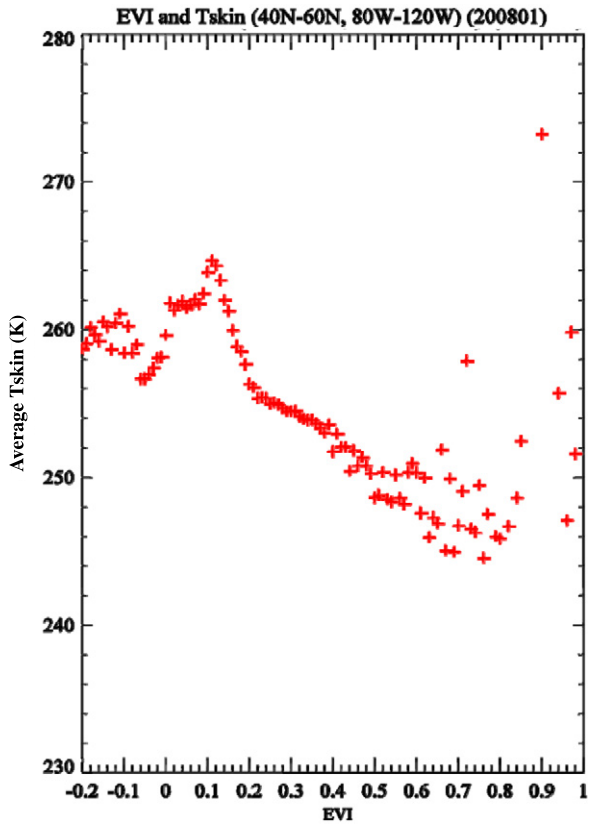

Figure 11. MODIS T_{skin} at daytime and vegetation index. Both are monthly data from Terra MODIS daytime (10:30 am).

5. Issues in constructing data sets for T_{skin}

Given the importance of land surface T_{skin}, why has this variable not been more widely used? For example, IPCC 2001 and 2007 used satellite sea surface temperature (SST) as evidence of global climate change, but did not use land T_{skin}. There appear to be three major reasons that have hampered the use of T_{skin} in global climate change studies.

First, uncertainties in the T_{skin} data set limit its use. T_{skin} can be measured through microwave or thermal infrared channels. Remotely sensed T_{skin} is now widely available due in part to a larger suite of satellites providing these measurements, and due in part to improvements in the recovery of T_{skin} and its accuracy (e.g., Prata *et al* 1995, Schmugge *et al* 1998). Nevertheless, the uncertainty in detection of changes in this variable may be large enough to obscure actual change.

To retrieve T_{skin}, it is necessary to calculate atmospheric radiative transfer in order to account for atmospheric emission and molecular absorption. Even in the most transparent spectral windows, atmospheric emission and attenuation are not negligible, thus corrections are usually required. These corrections are best accomplished by incorporating atmospheric profile information, for example, through the use of radiosonde measurements in the radiative transfer model calculations. Such measurements, however, are time consuming and rarely available for extensive areas or time periods. For example, within the seven wavelengths that MODIS used to retrieve T_{skin}, where most thermal infrared remote sensing measurements operate, carbon dioxide (CO_2) and water vapor (H_2O) are the chief atmospheric components that attenuate radiation. The mixing ratio of CO_2 is nearly

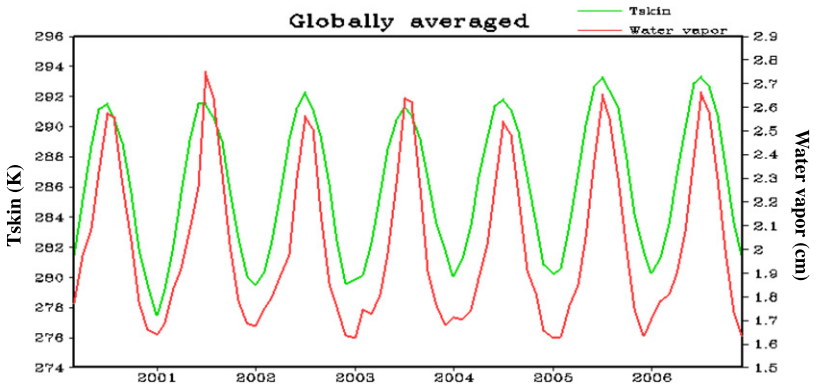

Figure 12. Global land surface averaged skin temperature versus water vapor. The data is based on MODIS monthly measurements from Terra (April 2000–December 2006).

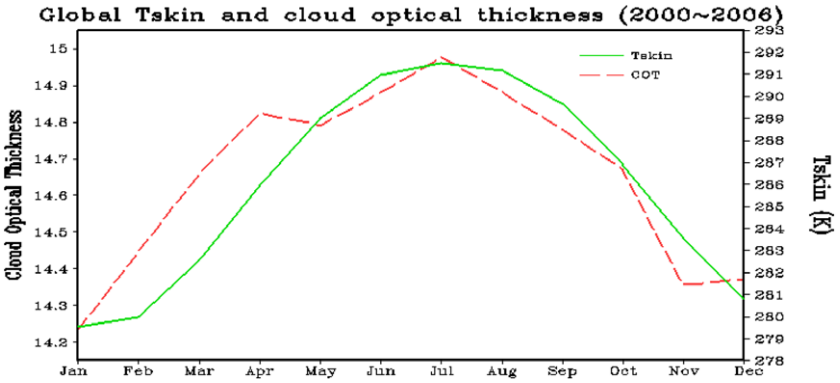

Figure 13. MODIS observed land surface T_{skin} versus cloud optical thickness (COT), averaged for April 2000–December 2006.

constant and thus not difficult to correct for. Water vapor is highly variable, however, and correcting for its effect may be difficult over an area of greater than a few kilometers or time periods greater than a few hours (Goody and Yung 1989).

Because of the high heterogeneity of the land surface, surface emissivity is largely unknown and thus induces a substantial uncertainty in the final retrieval. Atmospheric absorption increases with view angle and so also the retrieved values of skin temperature (Francois *et al* 1997). Instrument noise and variability are additional sources of error (Prata *et al* 1995), and limitations linked to the instrument itself also need to be recognized.

Second, satellite footprints cover a heterogeneous surface even for fine resolution of MODIS (1 km); its pixels in fact commonly contain several different land types. Thus, the interpretation of T_{skin} from satellite instruments, and its linkage to models or traditional measurements continues to be difficult.

Third, is the issue of the short duration of large-scale T_{skin} data sets. Evidence for climate change requires consistent, reliable, long-term data sets, but T_{skin} measurements first began at the end of the 1970s, and the changes of instrument and orbit drift have made construction of long-duration datasets problematical (Jin 2004).

6. Concluding remarks

Satellite observations, for example, MODIS data, have strengths such as high spatial and temporal resolutions, global coverage, and high quality. Therefore, satellite data are very useful for studies on land surface climate. The most advanced satellite observations show that:

(1) T_{skin} is clearly a different physical parameter from T_{air}.
(2) Land surface skin temperature is determined by both land surface properties and atmosphere interactions (water vapor, clouds, etc).
(3) Scale is critical for understanding T_{skin} and its interactions with land surface and the overlying atmosphere.

This letter shows T_{skin} data on the monthly scale, and relates it to T_{air}, to water vapor and to clouds. Different features would be expected at smaller spatial and temporal scales. Improved climatological data sets of T_{skin} could provide considerable benefits. The climatologies of T_{air} are designed primarily to examine long-term and large-scale changes. However, such changes may not be ideal for the study of the predominantly local and regional impacts of climate change. Also, T_{skin} may be more directly connected to systems impacted, such as canopies.

Both the T_{skin} versus land cover and T_{skin} versus albedo relationships show that in addition to the changes in air temperature and insolation, T_{skin} also depends on vegetation health, canopy depth, and soil wetness. Because of such interdependencies, it may be difficult to relate the changes in T_{skin} to one specific physical process.

More field measurements of T_{skin}, together with T_{air} and surface and atmosphere conditions would improve the

understanding and modeling of this quantity. The most widely used T_{skin}-included field experiments are still the First ISLSCP Field Experiment (FIFE, Sellers *et al* 1992), the Boreal Ecosystem-Atmosphere Study (BOREAS, Sellers *et al* 1997), and the Atmospheric Radiation Measurement (ARM, Xie *et al* 2010). New carefully designed and implemented field experiments over various land covers would be extremely valuable to validate satellite and model simulations or to examine T_{skin} and T_{air} relationships.

MODIS skin temperature is retrieved for clear days only, which is a limitation of MODIS land skin temperature observations due to the fact that MODIS only uses IR channels to retrieve surface temperature, and therefore cannot see through clouds. When clouds are present at the satellite overpass time, the satellite cannot observe skin temperature. As a result, all the diurnal, seasonal, and interannual variations presented in this paper are for clear days. How to convert the clear-day data into whole-sky data (clear and cloudy) is a challenging research topic (Jin and Dickinson 1999, 2002). Furthermore, when climate modelers compare model output with MODIS skin temperatures, satellite limitations need to be kept in mind.

Skin temperatures retrieved from satellite give information about the ground temperature of bare soils, if there is bare soil presented in the field of view of satellite instrument. After the removal of the atmosphere effect, radiances coming from the field of view of the instrument are a combination of the underlying bare soil and vegetation. A skin temperature for one pixel is therefore the average of the effective temperature of the pixel. Similarly, in a land surface model, for a grid box partially covered by bare soil and partially covered by vegetation, skin temperature of the grid is the sum of canopy top temperature and ground temperature weighted by their fractions (Dickinson *et al* 1986).

Skin temperature, as shown in equations (2) and (3), is critical in calculating heat transfer from land surface to atmosphere (Beljaars and Holtslag 1991, Choudhury *et al* 1986, Jin and Liang 2006). Nevertheless, this is not the focus of this letter. How to use skin temperature to calculate surface fluxes will be an important ongoing research topic. Remote sensing scientists have made some progress but their results are limited by the uncertainty of their approaches for broader applications (Nemani *et al* 2001).

Acknowledgments

This work is funded by the NSF Atmosphere Program through grant ARARD no ATM 0855480 and the NASA Precipitation Program through grant award no NNX07AF39G.

References

Anding D and Kauth R 1970 Estimation of sea surface temperature from space *Remote Sens. Environ.* **1** 217–20

Becker F and Li Z 1995 Surface temperature and emissivity at various scales: definition, measurement and related problems *Remote Sens. Rev.* **12** 225–53

Beljaars A C M and Holtslag A A M 1991 Flux parameterization over land surface for atmospheric models *J. Appl. Meteorol.* **30** 327–41

Choudhury B J, Reginato R J and Idso S B 1986 An analysis of infrared temperature observations over wheat and calculation of latent heat flux *Agric. Forest Meteorol.* **37** 75–88

Coll C, Caselles V and Schmugge T J 1994 Estimation of land surface emissivity differences in the split-window channels of AVHRR *Remote Sens. Environ.* **48** 127–34

Dickinson R E, Henderson-Sellers A and Kennedy P J 1993 Biosphere-atmosphere transfer scheme (BATS) version 1e as coupled to the NCARCommunity Model *NCAR Tech. Note NCAR/TN-387+STR* p 72

Dickinson R E, Henderson-Sellers A, Kennedy P J and Wilson M F 1986 Biosphere ± atmosphere transfer scheme (BATS) for the NCAR Community Climate Model *NCAR Technical Note NCAR/TN-275STR*

Francois C, Ottle C and Prevot L 1997 Analytical parameterization of canopy directional emissivity and directional radiance in the thermal infrared. Applications on the retrieval of soil and foliage temperatures using two directional measurements *Int. J. Remote Sens.* **18** 2587–621

Free M, Angell J K, Durre I, Lanzante J, Peterson T C and Seidel D J 2004 Using first differences to reduce inhomogeneity in radiosonde temperature datasets *J. Clim.* **21** 4171–9

Friedl M A *et al* 2002 Global land cover mapping from MODIS: algorithms and early results *Remote Sens. Environ.* **83** 287–302

Gao B-C, Yang P, Guo G, Park S K, Wiscombe W J and Chen B 2003 Measurements of water vapor and high clouds over the Tibetan Plateau with the Terra MODIS instrument *IEEE Trans. Geosci. Remote Sens. Lett.* **41** 895–900

Gao F, Schaaf C, Strahler A, Roesch A, Lucht W and Dickinson R 2005 The MODIS BRDF/Albedo climate modeling grid products and the variability of albedo for major global vegetation types *J. Geophys. Res.* **110** D01104

Garratt J R 1992 *The Atmospheric Boundary Layer* (London: Cambridge University Press)

Goody R M and Yung Y L 1989 *Atmospheric Radiation—Theoretical Basis* 2nd edn (New York: Oxford University Press)

Holmes R M 1969 Airborne measurements of thermal discontinuities in the lowest layers of the atmosphere *Paper Presented at 9th Conf. Agric. Meteorol. (Seattle, WA)* p 18

Huband N D S and Monteith J L 1986 Radiative surface temperature and energy balance of a wheat canopy *Bound. Layer Meteorol.* **36** 1–17

Jin M 2004 Analyzing skin temperature variations from long-term AVHRR *Bull. Am. Meteorol. Soc.* **85** 587–600

Jin M and Dickinson R E 1999 Interpolation of surface radiation temperature measured from polar orbiting satellites to a diurnal cycle. Part 1: without clouds *J. Geophys. Res.* **104** 2105–16

Jin M and Dickinson R E 2002 New observational evidence for global warming from satellite data *Geophys. Res. Lett.* **29** 39

Jin M, Dickinson R E and Vogelmann A M 1997 A comparison of CCM2/BATS skin temperature and surface-air temperature with satellite and surface observations *J. Clim.* **10** 1505–24

Jin M, Dickinson R E and Zhang D-L 2005 The footprint of urban areas on global climate as characterized by MODIS *J. Clim.* **18** 1551–65

Jin M and Liang S 2006 An improving land surface emissively parameter of land surface models using global remote sensing observations *J. Clim.* **19** 2867–81

King M D, Menzel W P, Kaufman Y J, Tanré D, Gao B C, Platnick S, Ackerman S A, Remer L A, Pincus R and Hubanks P A 2003 Cloud and aerosol properties, percipitable water, and profiles of temperature and humidity from MODIS *IEEE Trans. Geosci. Remote Sens.* **41** 442–58

Li Z-L and Becker F 1993 Feasibility of land surface temperature and emissivity determination from AVHRR data *Remote Sens. Environ.* **43** 67–86

Nemani R R, White M A, Cayan D R, Jones G V, Running S W and Coughlan J C 2001 Asymmetric warming over coastal California and its impact on the premium wine industry *Clim. Res.* **19** 25–34

Norman J M and Becker F 1995 Terminology in thermal infrared remote sensing of nature surfaces *Agric. Forest Meteorol.* **77** 153–66

Oke T R 1987 *Boundary Layer Climates* 2nd edn (London: Methuen)

Oleson K W *et al* 2008 Improvements to the community land model and their impact on the hydrological cycle *J. Geophys. Res.* **113** G01021

Peterson T C, Karl T R, Jamason P F, Knight R and Easterling D R 1998 The first difference method: maximizing station density for the calculation of long-term global temperature change *J. Geophys. Res. Atmos.* **103** 25967–74

Peterson T C and Russell S V 1997 An overview of the global historical climatology network temperature data base *Bull. Am. Meteorol. Soc.* **78** 2837–49

Platnick S, King M D, Ackerman S A, Menzel W P, Baum B A, Riédi J C and Frey R A 2003 The MODIS cloud products: algorithms and examples from Terra *IEEE Trans. Geosci. Remote Sens. Lett.* **41** 459–73

Prata A J 1993 Land surface temperatures derived from the advanced very high resolution radiometer and the along-track scanning radiometer: 1. Theory *J. Geophys. Res.* **98** 16689–702

Prata A J, Caselles V, Colland C, Sobrino J A and Ottle C 1995 Thermal remote sensing of land surface temperature from satellites: current status and future prospects *Remote Sens. Rev.* **12** 175–224

Price J C 1984 Land surface temperature from measurements from the split window channels of the NOAA 7 advanced very high resolution radiometer *J. Geophys. Res.* **89** 7231–7

Saunders P M 1967 Aerial measurements of sea surface temperature in the infrared *J. Geophys. Res.* **72** 4109–17

Schaaf C B *et al* 2002 First operational BRDF, Albedo and Nadir reflectance products from MODIS *Remote Sens. Environ.* **83** 135–48

Schmugge T J and Becker F 1991 Remote sensing observations for the monitoring of land-surface fluxes and water budgets *Land Surface Evaporation: Measurements and Parameterization* ed T J Schmugge and J C Andre (New York: Springer)

Schmugge T J, Hook S J and Coll C 1998 Recovering surface temperature and emissivity from thermal infrared multispectral data *Remote Sens. Environ.* **65** 121–31

Sellers P J, Hall F G, Asrar G, Strebel D E and Murphy R E 1992 An overview of the first international satellite land surface climatology project (ISLSCP) field experiment (FIFE) *J. Geophys. Res.* **97** 18345–71

Sellers P J *et al* 1997 The Boreal Ecosystem-Atmosphere Study (BOREAS): an overview and early results from the 1994 field year *Bull. Am. Meteorol. Soc.* **76** 1549–77

Sobrino J A, Li Z L, Stoll M P and Becker F 1994 Improvements in the split-window technique for land surface temperature determination *IEEE Trans. Geosci. Remote Sens. Lett.* **32** 243–53

Stephens G L 1994 *Remote Sensing of the Lower Atmosphere: An Introduction* (Oxford: Oxford University Press)

Sun J and Mahrt L 1995 Determination of surface fluxes from the surface radiative temperature *Atmos. Sci.* **52** 1096–106

Ulivieri C, Castronuovo M M, Francioni R and Cardillo A 1994 A split window algorithm for estimating land surface temperature from satellites *Adv. Space Res.* **14** 59–65

Wan Z 2008 New refinements and validation of the MODIS land-surafce temperature/emissivity products *Remote Sens. Environ.* **112** 59–74

Wan Z and Dozier J 1996 A generalized split-window algorithm for retrieving land-surface temperature from space *IEEE Trans. Geosci. Remote Sens. Lett.* **34** 892–904

Wan Z and Li Z-L 2008 Raidance-based validation of the V5 MODIS land-surface temperature product *Int. J. Remote Sens.* **29** 5373–95

Xie S *et al* 2010 ARM climate modeling best estimate data: a new data product for climate studies *Bull. Am. Meteorol. Soc.* **91** 13–20